Neural Network Approximations of the Temperature of CdTe Quantum Dots

Charles Lewis

A senior thesis submitted to the faculty of
Brigham Young University
in partial fulfillment of the requirements for the degree of

Bachelor of Science

John Colton, Advisor

Department of Physics and Astronomy

Brigham Young University

ABSTRACT

Neural Network Approximations of the Temperature of CdTe Quantum Dots

Charles Lewis
Department of Physics and Astronomy, BYU
Bachelor of Science

Various biological processes require accurate temperature sensing through microfluidic devices, so improved temperature sensors methods are needed. Previously, machine learning techniques have been used for predicting temperatures through thermal images. To develop a new, accurate temperature sensor model, photoluminescence (PL) spectra and time-resolved photoluminescence (TRPL) spectra of CdTe quantum dots were measured as functions of temperature for use in training an artificial neural network (ANN). A low-temperature regime from 10-300 K and a high-temperature regime from 298-319 K were measured with additional data provided through interpolation. The optimized neural network is able to determine temperatures with a mean average error of 7.7 K and 0.1 K for the low and high-temperature regimes respectively. The mean absolute error of the low-temperature regime improves to 0.4 K when restricting to temperatures between 100-300 K.

Keywords: machine, learning, neural, network, temperature, sensor, nanoparticle, quantum, dot, resonant, cavity

ACKNOWLEDGMENTS

I would like to acknowledge my many professors who have taught me important principles of different areas of physics. I would also like to extensively thank Dr. John Colton, who has given vast amounts of time to advise and mentor me. I have learned a great deal from him through classroom instruction, group meetings, and individual interactions. None of this would have been possible without his help and guidance.

Contents

List of Figures

Chapter 1

Introduction

1.1 Quantum Dots

Quantum dots are tiny semiconductor particles that have optical and electrical properties that differ from larger particles due to quantum mechanics. Their unique properties can be useful in photovoltaic and light emitting devices in addition to bioimaging. They display unique electronic properties, intermediate between those of bulk semiconductors and discrete molecules, that are partly the result of the unusually high surface-to-volume ratios for these particles. The most apparent result of this is photoluminescence, wherein the nanocrystals can produce distinct colors determined by the size as well as the composition of the particles. The cadmium telluride quantum dots used in this experiment are nanosized spheres with a diameter of about 2 to 10 nm.

Quantum dots are particularly significant for optical applications owing to their bright colors coupled with their high efficiencies, longer lifetimes and high extinction coefficient [1]. Examples include LEDs and solid state lighting, displays and photovoltaics. The small size of these quantum dots allow them to go anywhere in the body making them suitable for different bio-medical applications like medical imaging and biosensors. At present, fluorescence based biosensors depend

on organic dyes with a broad spectral width, which limits their effectiveness to a small number of colors and shorter lifetimes. On the other hand, quantum dots can emit the whole spectrum, are brighter and have little degradation over time thus proving them superior to traditional organic dyes used in biomedical applications [2].

1.2 Temperature Sensors

Accurate temperature sensing is needed in many biological processes. The requirements for a biothermal sensor are stringent because the sensor has to meet requirements relating to biocompatibility, small probe size, rapid sensor response, and the ability to provide spatial information on temperature [3] [4]. One of the few available options for temperature sensing that fit these criteria is a microfluidic device. A microfluidic device is a device used to analyze a tiny amount of liquid, smaller than a droplet. These devices have microchannels ranging from submicron to a few millimeters in size for precision in controlled experiments. Typical biothermal sensing devices used in microfluidic devices include IR and Raman thermography, thermocouples and platinum resistance temperature detectors, liquid crystals, nano and bulk diamonds, fluorescent dyes, proteins, and quantum dots. Current technologies for temperature sensing through microfluidic devices are lacking since their accuracy is limited to about 1 K over a temperature range of tens of degrees. [5]. The motivation for this project is to improve the temperature sensing accuracy and range of microfluidic devices by developing a machine learning model for predicting temperature.

1.3 Machine Learning

Machine learning is an application of artificial intelligence that provides systems the ability to automatically learn and improve from training in a way that is generalized. Applied to data analysis, machine learning can automate analytical model building. Historically, the focus of machine learning

via neural networks for thermal application has been on image recognition in thermal images [6] [7]. These instances of temperature sensors benefiting from machine learning demonstrate the potential to improve temperature sensing in biological system through the utilization of neural networks in the interpretation of temperature sensitive signals.

For classifying the temperature based on the data of these temperature sensitive signals, we chose to use artificial neural networks as our model. Artificial neural networks (ANN) are a set of machine learning algorithms modeled loosely after the human brain. They consist of a number of interconnected artificial neurons, otherwise known as nodes, contained in layers and then connected in series. Each node takes a weighted linear combination of the outputs from nodes of the previous layer, applies some non-linear "activation function", and then outputs the result to the next layer.

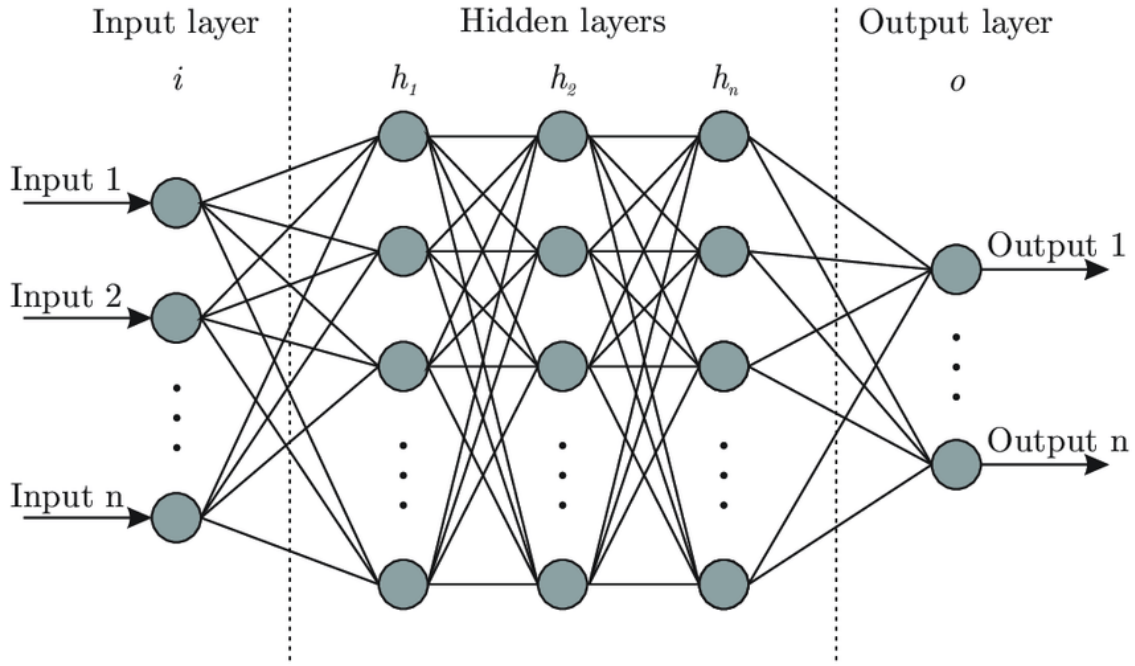

Figure 1.1 The data is fed into the input layer of neurons and then passed through hidden layers where each neuron of one layer connects to each neuron of the following layer until the output layer. Every neuron has a weight attached with a positive or a negative value. The neuron sums all the signals it receives, with each signal being multiplied by its associated weights on the connection. The data is then passed through an activation function to give the final output. From Ref. [8]

The difference between the predicted and real outputs is described as a "loss" function, L, for example the mean squared error between real and predicted. An algorithm modifies the weights associated with each node so that the loss function decreases as training progresses.

1.4 Prior Work at BYU

In previous work, our group (the research group of Dr. John Colton at Brigham Young University) demonstrated that improved data analysis of quantum dot fluorescence by machine learning improved the temperature prediction accuracy for temperature sensors from ± 1.0 to ± 0.3 degrees Kelvin over a range of 300-312 K. To accomplish this, several spectral features of quantum dots such as the absolute intensity of the fluorescent peak, the wavelength of the peak emission, and the normalized intensity of the fluorescent spectra at several spectral bands were used as inputs to a neural network. The network was then trained to relate the spectral features to the temperatures measured with a calibrated platinum resistance temperature detectors. We also achieved accuracies near ± 0.6 degrees K at times as short as 10 ns. These approaches required the use of absolute values of peak intensity, so the accuracy of the approach was only applicable to that particular application.

1.5 Thesis Overview

Our group performed this research in hopes of creating a more general approach that can be applied over a larger range of temperatures than previously done for biothermal sensing in microfluidic devices. Accordingly, the overall goal of this research consisted in creating a new machine learning model to accurately predict temperatures by means of a neural network trained on photoluminescence data of cadmium telluride quantum dots. Much of the experimental methods and results of this research has been recently accepted for publication in the ACS Applied Nanomaterials journal. Upon future publication, the paper will be found under the title "Use of Machine Learning with

Temporal Photoluminescence Signals from CdTe Quantum Dots for Temperature Measurement in Microfluidic Devices". This thesis gives a general introduction and background in the first chapter, the experimental methods and training of the neural network in the second chapter, and the results and summary in the third chapter.

Chapter 2

Experimental Methods for Temperature Sensors

In outlining the process of creating a machine learning model for predicting temperatures, this chapter describes the creation of a microfluidic device and explains the setup of the experiment for gathering photoluminescence data with the CdTe quantum dots in the microfluidic device. The interpolation method used for generating additional data is presented. Also, the development and optimization of the neural networks used to predict temperatures corresponding to the input optical data is discussed.

2.1 Microfluidic Device

A microfluidic device was created to hold the CdTe quantum dots in place. This device was designed using an open source CAD software and printed on an Asiga 3D printer with PR48 resin. The printed device was 12mm $\times$ 12mm $\times$ 4mm with two parallel 1mm $\times$ 1mm channels for housing the quantum dots and a heating material. The PR48 resin was impregnated with CdTe quantum dots via sonication, injected into the device, and cured in place through a thermal baking process [5]. The

device also had an additional channel to get the thermocouple as close as possible to the embedded CdTe quantum dots during the high-temperature measurements. A picture of the device created is included in Fig 2.1. Copper wires were placed in the external openings of the heating channel and the channel was sealed off. These copper wires were the access points for the DC power source used for the heating.

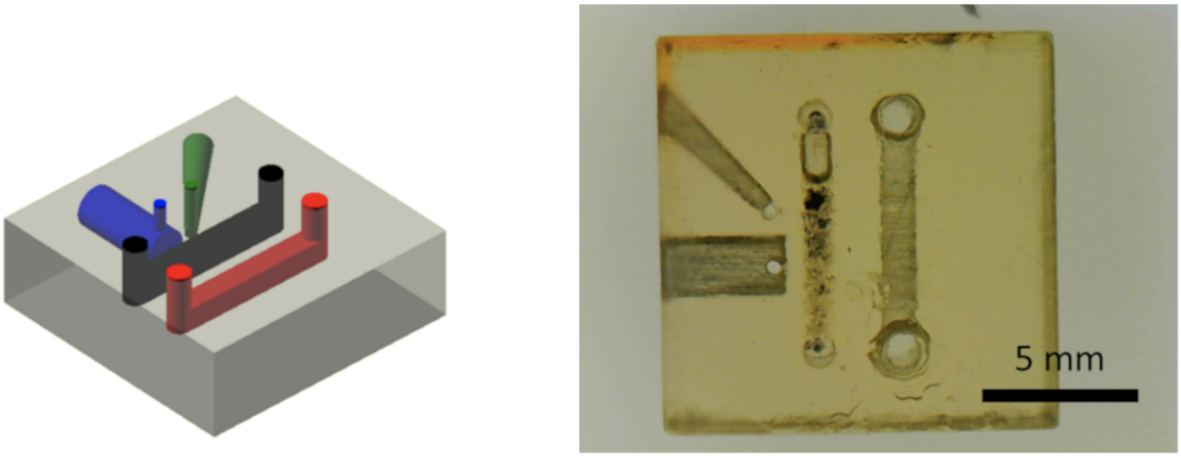

Figure 2.1 CAD model sent to printer and PR48-resin printed device with CdTe impregnated PR48 resin filling channels.

2.2 Experimental Setup and Optical Data

Photoluminescence (PL) is the light emission that occurs from the process in which a material absorbs a photon in the visible spectrum, exciting one of its electrons to a higher electronic excited state, and then radiates a photon as the electron returns to a lower energy state. Time periods between the absorption and the emission may vary, even ranging from femtoseconds to milliseconds and possibly to minutes or longer [4]. Time-resolved photoluminescence (TRPL) is a method where the sample is excited with a light pulse, and then the decay in photoluminescence with respect to time is measured. By observing how long individual molecules take to emit their photons, and then combining all these data points, an intensity vs. time graph can be generated that displays the

exponential decay curve typical to these processes.

The CdTe quantum dot samples were sealed into PR48 resin chips and brought to the desired temperature points by a commercial cryostat for low temperatures or a custom PID controller for high temperatures. The PID controller measures temperature with a thermocouple and drives a the galinstan heating element embedded into the PR48 chip. Both wavelength and delay time curves display changes with temperature; therefore, optical data calibrated for temperature can be used to create an optical temperature probe [5].

For taking the PL and TRPL data, a laser excited photoluminescence from the sample, which was either on a cryostat or on a heating stage. The PL was collected and focused onto a spectrometer. The spectrometer then analyzed the PL for wavelength dependence using a photomultiplier tube (PMT) detector or CCD detector for PL spectra. For time-resolved PL, a pulse generator sent a signal to the laser and to the start signal to the TCSPC module as shown in Fig 2.2. The spectrometer was set to the peak wavelength while the PMT signal triggered the TCSPC module to stop. For additional information on the experimental setup and methods, see the senior thesis of James Erikson titled, "Photoluminescence Lifetime as an Indicator of Temperature in Materials. [9]

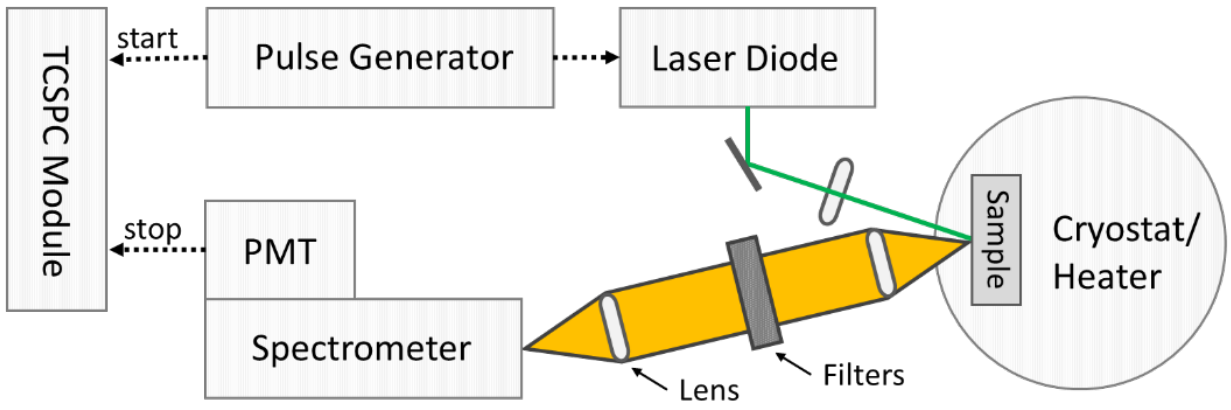

Figure 2.2 Optical experimental setup.

The time-resolved PL was measured with the technique of time-correlated single photon counting

(TCSPC). TCSPC measures the time delay between PL excitation and PL emission. A timing module started when it receives a trigger from a laser pulse, then stopped upon the detection of a photon from PL. This measurement was repeated many times and the time values obtained were used to create a histogram. Since the time scale of the decay approached the time limitations of the system, this measured data was not representative of the sample's actual PL lifetime decay. An instrument response function (IRF) was obtained since the measured TCSPC data was the convolution of the IRF with the actual TRPL. The standard method of characterizing the decay is to assume a functional form for the actual decay using several parameters and then do an iterative reconvolution fit where the difference between the measured data and the convolution is minimized as the parameters are varied [5]. The fit was performed to find the true TRPL of the CdTe quantum dots.

PL spectral and TCSPC data were taken in both a low-temperature and a high-temperature regime. The low temperatures range from 10 to 300 K in increments of 10 K, and the high temperatures range from 298 to 319 K in increments of 1 K. Representative PL spectra and time-resolved PL data are shown in Fig 2.2.

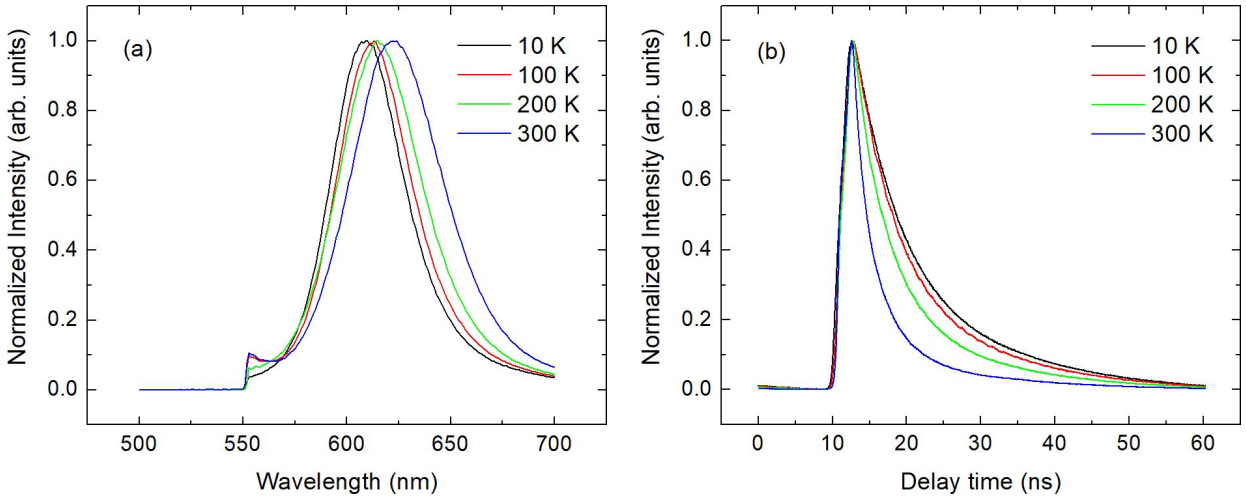

(a) PL spectral data **(b)** TCSPC data

Figure 2.3 Example PL spectral and TCSPC data from 10, 100, 200, and 300 K. Both intensities are normalized so the minimum value is 0 and the maximum value is 1. The peak in in normalized intensity shifts to the right for higher temperatures in the PL spectral data while the exponential curve drops off more quickly for higher temperature in the TCSPC data. These temperature defining features are more evident with higher temperatures.

The PL spectral data and the TCSPC data were concatenated as inputs for the machine learning. Thus the NN input data had a length of 2613 and 2605 for the low and high-temperature regimes respectively. Details on the optical data files used in the machine learning are provided in Table 2.1. In the final ANN, a (0, 1) min-max normalization on each dataset was used because the absolute intensity, while temperature dependent, is considerably dependent on experimental factors such as specific detectors, optical alignment, and geometry which varies heavily from one laboratory to another [5]. This normalization did cause the absolute PL intensity to be lost as potential learning feature, since the PL intensity correlates quite strongly with temperature. However, with the normalization, machine learning results obtained should provide a more representative idea of what can be achieved by training a network with data obtained in in one laboratory and later applying it to optical measurements (i.e. the inputs for the trained machine learning model) performed in a different place.

Table 2.1 Details of data files of optical measurements used in the machine learning

Optical Measurement	Scan Range	Step Size	Number of Points
Low-temperature spectrum	500-700 nm	1.000 nm	201
High-temperature spectrum	500-700 nm	1.041 nm	193
TCSPC	0-60.275 ns	0.025 ns	2412

2.3 Data Augmentation through Interpolation

Because of the limited number of data samples, the training data is supplemented with additional data through augmentation to increase the overall accuracy of the model. Dataset augmentation, the practice of applying a wide array of domain-specific transformations to synthetically expand a training set, is a standard tool in machine learning [10]. For machine learning algorithms, more data means better results as long as the additional data offers more details into features while reducing noise, though this is only true if the data is mostly clear of noise itself. Several data augmentation methods exist to expand datasets and reduce overtraining, such as interpolation, extrapolation, random insertion or deletion, and general mathematical transformations. [11].

We chose interpolation to augment our data and approximate the PL and TCSPC data for temperatures between those that were measured. The additional training samples of PL spectral data and TCSPC data, shown in Figures 2.4 and 2.5, were generated by cubic interpolation from the measured data in steps of 1 K for the low-temperature regime and steps of 0.1 K for the high-temperature regime. All but five temperatures in each temperature regime, ten total, were used in the interpolation. These withheld temperatures were not included in interpolation to serve as a holdout dataset to assess the accuracy of the machine learning model after training. These ten temperatures were chosen pseudo-randomly with some human intervention so that no two withheld temperatures would be adjacent to each other. The low temperatures set aside include 70, 90, 120, 180, and 250 K, while the high temperatures set aside include 301, 305, 310, 313, and 316 K.

For training the final machine learning model, the TCSPC data was concatenated to the end of the PL spectral data producing arrays with lengths of 2613 and 2605 for the low and high-temperature regimes respectively. Since the interpolation for the low-temperature regime was in the range of 10 to 300 K in steps of 1 K, the full dataset available for machine learning yielded 291 temperatures with the pairs of normalized spectral and TCSPC data concatenated together. The interpolated dataset used for machine learning in the low-temperature regime is plotted in Figure 2.4.

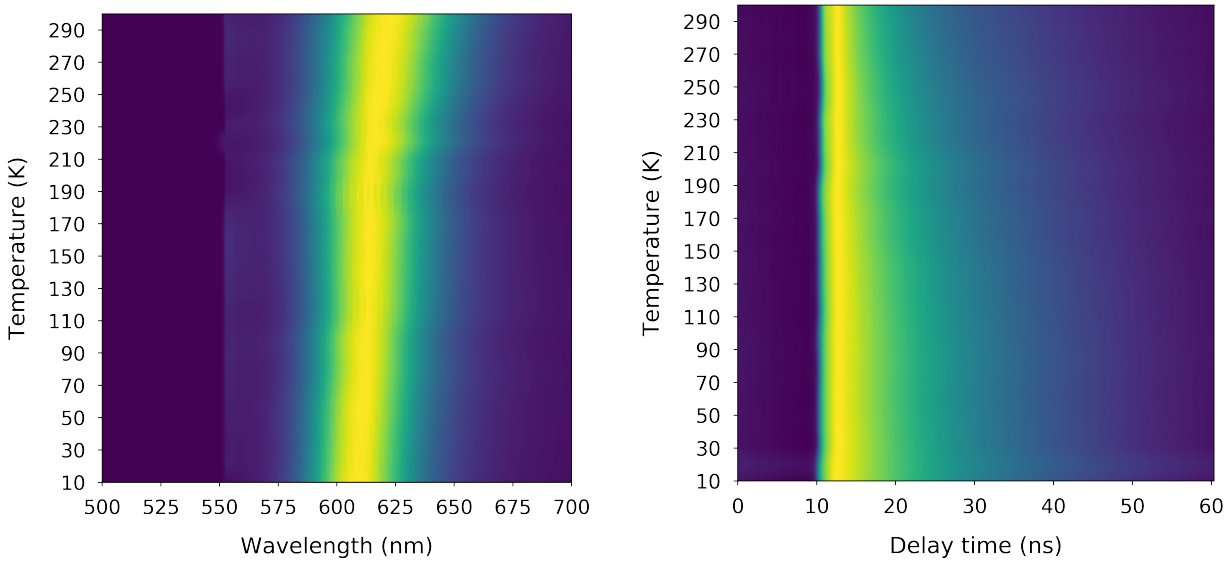

(a) PL spectral data **(b)** TCSPC data

Figure 2.4 The training data created from the cubic interpolation for the low-temperature regime. The color gradient corresponds to the min-max (0,1) normalized intensity in arbitrary units.

Since the interpolation for the high-temperature regime was in the range of 325 to 346 K in steps of 0.1 K, the full dataset available for machine learning yielded 211 temperatures with the pairs of normalized spectral and TCSPC data concatenated together. The interpolated, normalized dataset used for machine learning in the high-temperature regime is plotted in Figure 2.5.

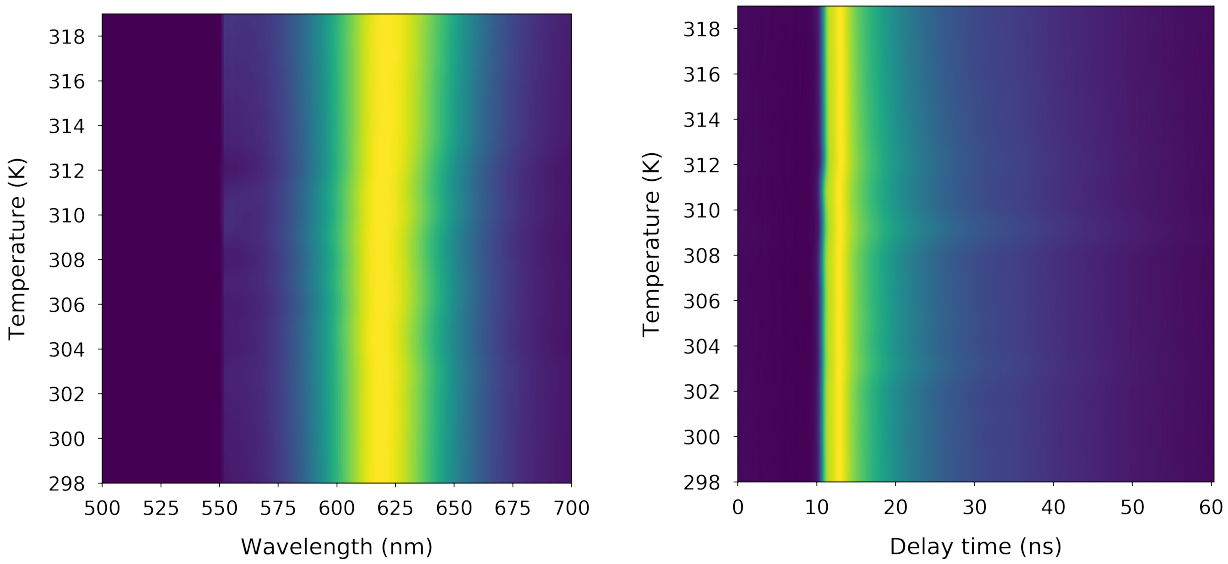

(a) PL spectral data **(b)** TCSPC data

Figure 2.5 The training data created from the cubic interpolation for the high-temperature regime. The color gradient corresponds to the min-max (0,1) normalized intensity in arbitrary units.

2.4 Data Preprocessing

Data preprocessing is a common machine learning procedure that is used to increase the ability of the model to learn as it improves the quality of data and the useful information that can be derived from it directly [12]. These preprocessing techniques can standardize, adjust, and highlight important features in the data before the data is processed by the machine learning model [13]. We explored several preprocessing techniques such as principle component analysis, methods of normalization, and natural logarithm transformations.

Principal component analysis (PCA) is a statistical procedure that uses an orthogonal transformation to convert a set of observations of possibly correlated variables (entities each of which takes on various numerical values) into a set of values of linearly uncorrelated variables called principal components []. PCA helps to reduce the dimensionality of a problem and speed up processing

time by removing features of the data that correlate poorly to the feature of interest. Advantages of feature elimination methods include simplicity and maintaining interpretability of the variables. This approach is particularly advantageous to neural networks as simplified data with clearer features is easier to model. However, the disadvantage is that no information is gained from the variables dropped. After testing several different models, PCA was determined to be unnecessary as all of the models performed worse with the reduced dimensionality, so PCA was not used in the final machine learning model.

Different normalization methods were tested as a preprocesing technique in improving the quality of the machine learning inputs by scaling the features of the PL spectral and TCSPC data to the same range. Min-max normalization was tested first and is used to linearly scale the data between 0 and 1. This linear transformation adjusted the values of the data without distorting the differences between them. This normalization creates smaller standard deviations in the data that can suppress the effects of outliers. Normalization with tanh estimators was also examined to improve the results for the high-temperature regime. Tanh estimators are useful because the data becomes even less sensitive to outliers and is more efficient than min-max normalization. Ultimately, min-max normalization was used in the final model since it provided the best results with the ten temperatures from the holdout dataset while also allowing anyone in the future to use the model, provided they normalize the data. Additionally, we also performed a natural log transformation on the TCSPC data before it was min-max normalized. Since the TCSPC data follows an exponential decay, taking the natural log first gives more weight to points on the decay at later times than they otherwise would have. [5]

2.5 Optimization of ANN

Overall, we tested many different types of neural network architectures for optimizing the model for investigating CdTe nanoparticles as non-invasive temperature sensors. Variations in the architecture related to the number of input branches, the number of layers, the number of nodes per layer, the activation functions, the duration of epochs trained (an epoch being one cycle through the full training data set), and the activation functions for each layer.

Different types of neural networks were tested and are defined as follows. A dense fully-connected neural network (DNN) is an artificial neural network with multiple, dense layers between the input and output where each neuron in one layer is connected to every neuron in another layer. A convolutional neural network (CNN) is a specific type of deep neural network that has built-in convolutional layers, which employ the mathematical operation of convolution in place of general matrix multiplication [15]. CNNs have historically been effective in image classification problems and in working with multi-dimensional data [6]. In the final machine learning model, the input array to the neural network was created by concatenating the PL spectral and TCSPC data and this is referred to as "input together". However, we also tested inputting the PL spectral and TCSPC data into separate branches of the neural network where the branches joined together after a few layers and this is referred to as "two input". Models were also created using only the PL spectra and only the TCSPC data as inputs to a DNN. In all of these architectures, the input data, whatever it is, goes into the NN and out of the NN comes a predicted temperature.

The different network architectures were trained in the same way using the Keras API in Python with TensorFlow backend. The training ran for 6000 epochs using an 80-20 training/testing split, where 80% of the data is used for training and 20% is used for testing. The testing dataset acts as an additional method for evaluating the effectiveness of the training, since the NN does not train on the testing data. The mean squared error of the model's predicted temperatures versus the actual temperatures was measured after each epoch for both the training and testing datasets. The

Table 2.2 Results of the mean absolute error (MAE) of the network's predicted temperatures compared to the true values for several architectures for the low-temperature regime

Architecture	MAE (K)
Two Input CNN	13.6
Input Together CNN	9.9
Two Input DNN	8.4
Spectra Only DNN	9.2
TCSPC Only DNN	11.3
Input Together DNN	7.7

"restore_best_weights" argument of the early stopping callback was set to true so that all models were compared with their best weights. The models' accuracy was determined by calculating the mean absolute error between the true temperatures and the predicted temperatures of the holdout dataset for the low-temperature regime. As shown in Table 2.2, the DNN with the PL spectral data concatenated into one input array with the TCSPC data performed best.

Thus, the optimal neural network architecture was chosen to be the input together DNN for the low-temperature regime. This DNN consisted of seven layers with (512, 256, 128, 64, 32, 16, 1) nodes in the corresponding layer. This DNN structure is shown in Fig 2.6 a. A grid-search method was employed to evaluate various hyperparameters of the DNN and determine the best learning rate, activation function, and optimizer. With the results of the grid search, the final model for the low-temperature regime was trained with a learning rate of 0.001, "Relu" activation functions for each layer, and the Adam optimizer [citation]. The model finished training with a mean absolute error of 0.1 K for the training data set, 0.3 K for the testing dataset, and 7.7 K for the holdout dataset. The DNN for the high-temperature regime was created using the same architecture and hyperparameters as the low-temperature regime, albeit with an array input length of 2605 due to

the slightly smaller PL spectral data file size. For the high-temperature regime, the model finished training with a mean absolute error of 0.1 K for the training data set, 0.2 K for the testing dataset, and 0.1 K for the holdout dataset.

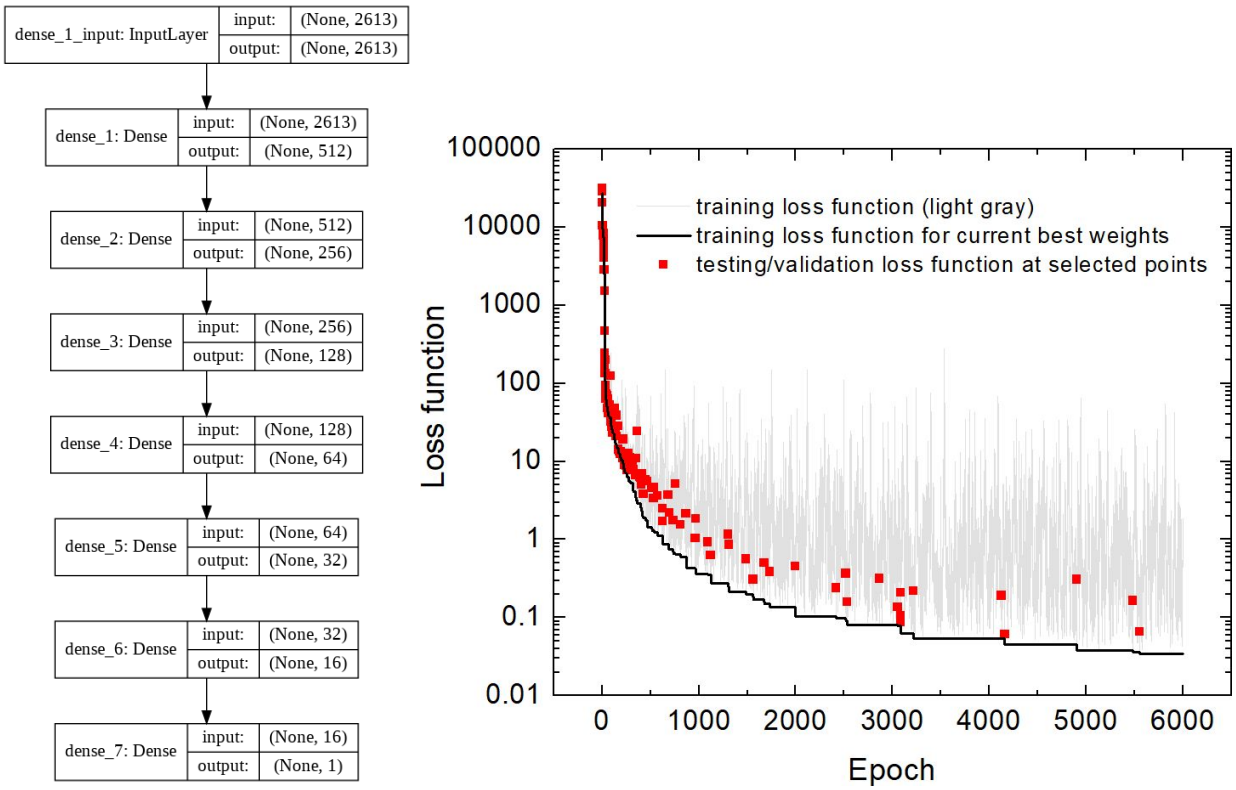

(a) Final NN architecture **(b)** Loss history

Figure 2.6 Architecture and loss history of the final optimized dense neural network for the low-temperature regime. Both the losses of the training and testing/validation datasets are plotted. The losses were updated for both datasets whenever the training reached a new minimum because the network was set to restore the best weights. The background shows the training loss updated every epoch.

Chapter 3

Results and Conclusions for Temperature Sensors

In accordance with the goal of creating a machine learning model to predict temperatures based on the photoluminescence data from CdTe quantum dots, this chapter discusses the results of the neural network with the holdout dataset and an analysis of the overall results of all datasets including additional testing with artificial noise. Additionally this chapter describes an overall summary of the project and the direction of future work of neural network approximations for temperature sensors with quantum dots.

3.1 Neural Network Predictions

The performance of each neural network was assessed via mean absolute error of a holdout set of data. For the low-temperature regime, the mean absolute error of a holdout set was 7.7 K (or 0.4 K when the holdout set was restricted to temperatures above 100 K). For the high-temperature regime, the accuracy was 0.1 K. The NN prediction temperatures are plotted in Fig 3.1 against their true values for each temperature in the training, testing/validation, and holdout datasets for both

Table 3.1 The true vs. the predicted temperatures for the holdout data for both the low and high-temperature regimes.

True Temperature (K)	Predicted Temperature (K)
70.0	83.88
90.0	66.68
120.0	120.42
180.0	179.96
250.0	250.78
301.0	300.15
305.0	304.80
310.0	310.07
313.0	312.92
316.0	315.95

temperature regimes.

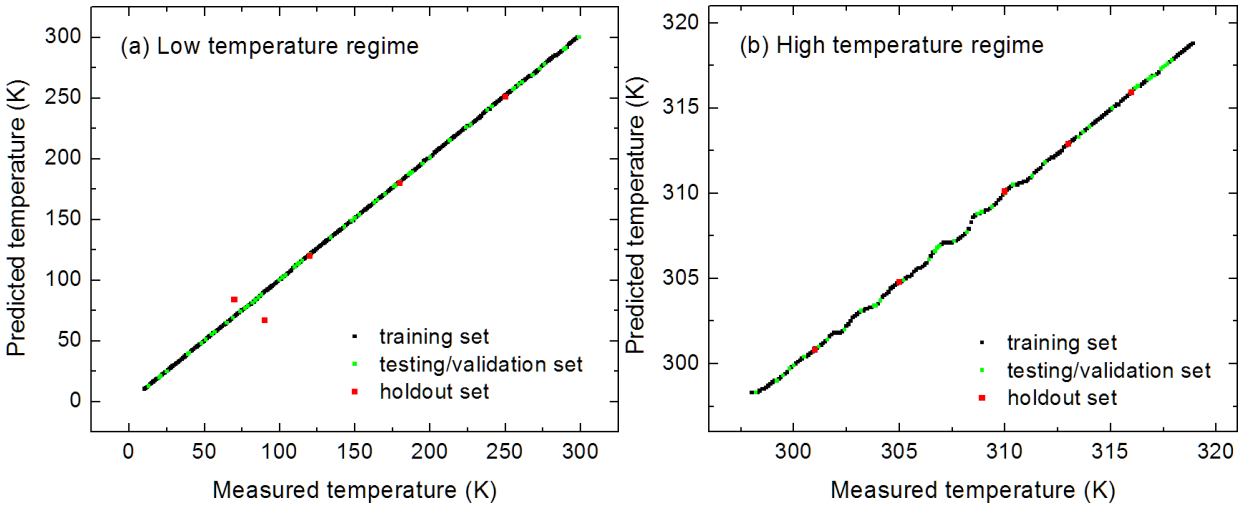

Figure 3.1 The predicted vs true temperature values for the training, testing/validation, and holdout sets. The training and testing/validation sets come from the 80-20 split of the training data. The holdout sets for each temperature regime consists of five points.

3.2 Analysis

The NN for the low-temperature regime performed poorly considering that the predictions for 70 and 90 K are both significantly off. A likely cause is that the photoluminescence spectra and the TCSPC data have little differences for the temperatures in the 10 to 100 K range. When looking at only the holdout data points in the 100-300 K range the NN gives a mean absolute error of 0.4 K. The reason for the large error at the holdout points of 70 and 90 K is probably related to the fact the optical properties change less per unit temperature at low temperatures than they do at higher temperatures, evident in the previous plots of PL and TCSPC data shown in Fig. 2.1. Both the PL spectral and TCSPC data change much more in the range of 200-300 K than they do in the range of 10-100 K. Thus, the classifying features that the neural network is able to identify are more apparent at higher temperatures giving more accurate predictions.

Additionally, the NN performed better with the high-temperature regime due to the smaller temperature interval between samples. Due to time constraints, optical data was taken every 10 K in the low-temperature regime compared to the 1 K interval for the high-temperature regime giving an overall narrower range of data for the high-temperature regime and allowing the NN to more accurately predict the temperature.

To provide a more comprehensive understanding of the performance of the NN in addition to the predictions of the holdout dataset, we also tested the effects of artificially added noise in the holdout data on the NN predictions. The noise for a given "percent noise added" value was sampled from a uniform distribution between negative and positive values of the percentage added. Accordingly, a 5 percent noise value means that random numbers between ± 0.05 of the maximum (or -0.05 and $+0.05$ since the data is normalized to a maximum of 1) were added as noise to the PL spectral or the TCSPC data. Evaluating the change in MAE was done 40 times for each "percent noise added" value, and means and standard deviations of the increase in MAE for the holdout data relative to the neural network predictions with no added noise were computed. The results are displayed in

Fig 3.2. For both temperature regimes, the neural networks were tolerant of noise to some degree, though a larger tolerance is displayed for noise added to the spectral data than noise added to the TCSPC data.

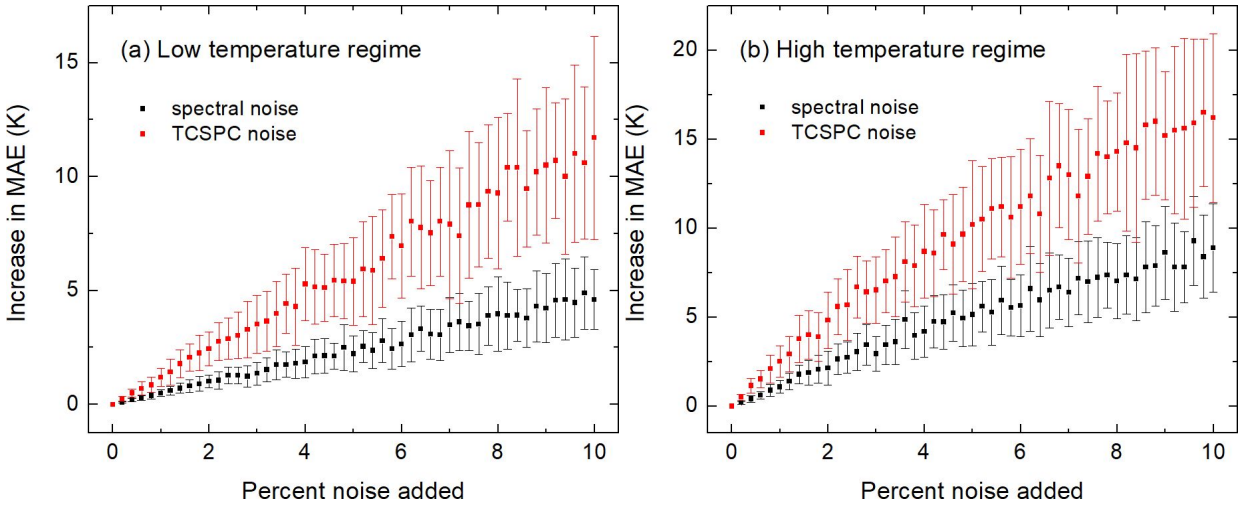

Figure 3.2 Additional evaluation of the neural network comparing the increase in the mean absolute error of predictions with noise artificially added to either the PL spectral or TCSPC holdout data after preprocessing.

3.3 Summary

A reliable machine learning model was obtained by using a combination of raw spectral joined with time-resolved PL data as the inputs. The inputs were min-max normalized, so intensity was not present as a learning feature, in order to be representative of what may occur when using different experimental systems for the training samples and the later use of the model. Interpolation was employed to increase the number of training samples by a factor of 10 for both temperature regimes. The samples were used to train a NN for approximating temperatures with a mean average error of 7.7 K and 0.1 K for the low and high-temperature holdout datasets respectively. The mean absolute error of the low-temperature regime improves to 0.4 K when restricting to temperatures between 100-300 K.

This current method for temperature sensing has a higher accuracy and wider range than many current biothermal sensing technologies. The implementation of this method could impact temperature sensing accuracy and resolution of microfluidic biothermal sensors and expand the number of temperature sensitive analyses possible without having to calibrate each microfluidic device separately.

3.4 Directions for Further Work

Shifts in the optical properties as a result of laser exposure or long term changes to the quantum dots can cause substantial changes to the temperature predictions, depending on the amount of change and the temperature regime. Thus, further work could be done to study the duration and accuracy over the time these CdTe quantum dots are viable for temperature sensing. Additionally, the project could be expanded to include different quantum dots in determining the most viable option for modern temperature sensing.

Bibliography

[1] L. Liu *et al.*, "Wideband fluorescence-based thermometry by neural network recognition: Photothermal application with 10 ns time resolution," Journal of Applied Physics **118,** 184906 (2015).

[2] S. Pandit, T. Banerjee, I. Srivastava, S. Nie, and D. Pan, "Machine Learning-Assisted Array-Based Biomolecular Sensing Using Surface-Functionalized Carbon Dots," ACS Sensors **4,** 2730–2737 (2019).

[3] A. T. Young, K. R. Rivera, P. D. Erb, and M. A. Daniele, "Monitoring of Microphysiological Systems: Integrating Sensors and Real-Time Data Analysis toward Autonomous Decision-Making,", 2019.

[4] G. Kucsko, P. C. Maurer, N. Y. Yao, M. Kubo, H. J. Noh, P. K. Lo, H. Park, and M. D. Lukin, "Nanometre-scale thermometry in a living cell," Nature **500,** 54–58 (2013).

[5] C. Lewis, J. W. Erikson, D. A. Sanchez, C. E. McClure, G. P. Nordin, T. R. Munro, and J. S. Colton, "Use of Machine Learning with Temporal Photoluminescence Signals from CdTe Quantum Dots for Temperature Measurement in Microfluidic Devices," ACS Applied Nano Materials (2020).

[6] G. Cerutti, R. Prasad, and E. Farella, "Convolutional Neural Network on Embedded Platform for People Presence Detection in Low Resolution Thermal Images," In *ICASSP, IEEE Inter-*

national Conference on Acoustics, Speech and Signal Processing - Proceedings, **2019-May,** 7610–7614 (Institute of Electrical and Electronics Engineers Inc., 2019).

[7] K. C. Lee, J. Siegel, S. E. Webb, S. Lévêque-Fort, M. J. Cole, R. Jones, K. Dowling, M. J. Lever, and P. M. French, "Application of the stretched exponential function to fluorescence lifetime imaging.," Biophysical journal **81,** 1265–74 (2001).

[8] F. Bre, J. M. Gimenez, and V. D. Fachinotti, "Prediction of wind pressure coefficients on building surfaces using artificial neural networks," Energy and Buildings **158,** 1429–1441 (2018).

[9] J. Erikson, Ph.D. thesis, Brigham Young University, 2020.

[10] T. DeVries and G. W. Taylor, "Dataset augmentation in feature space," In *5th International Conference on Learning Representations, ICLR 2017 - Workshop Track Proceedings*, (International Conference on Learning Representations, ICLR, 2019).

[11] A. Mikołajczyk and M. Grochowski, "Data augmentation for improving deep learning in image classification problem," In *2018 International Interdisciplinary PhD Workshop, IIPhDW 2018*, pp. 117–122 (Institute of Electrical and Electronics Engineers Inc., 2018).

[12] M. Stewart, "Neural Network Optimization - Towards Data Science,", 2019.

[13] P. Sane and R. Agrawal, "Pixel normalization from numeric data as input to neural networks: For machine learning and image processing," In *Proceedings of the 2017 International Conference on Wireless Communications, Signal Processing and Networking, WiSPNET 2017*, **2018-Janua,** 2221–2225 (Institute of Electrical and Electronics Engineers Inc., 2018).

[14] "Artificial neural network architecture (ANN i-h 1-h 2-h n-o). | Download Scientific Diagram,".

[15] A. Kwasigroch, A. Mikołajczyk, and M. Grochowski, "Deep convolutional neural networks as a decision support tool in medical problems – malignant melanoma case study," In *Advances in Intelligent Systems and Computing*, **577,** 848–856 (Springer Verlag, 2017).

Index